

*Numerical Evaluation of the Steel Plate
Energy Absorption Device (SPEAD)
for Seismic Strengthening of RC Frame
Structures*

**Giuseppe Santarsiero, Vincenzo
Manfredi & Angelo Masi**

**International Journal of Civil
Engineering**

ISSN 1735-0522
Volume 18
Number 8

Int J Civ Eng (2020) 18:835-850
DOI 10.1007/s40999-020-00510-x

Numerical evaluation of the Steel Plate Energy Absorption Device (SPEAD) for Seismic Strengthening of RC Frame Structures

Keywords: reinforced concrete; beam-column joint; seismic upgrading; energy absorption; finite element analysis

Abstract

In this paper, a new strengthening technique is proposed: the SPEAD (Steel Plate Energy Absorption Device) system, which is intended to increase the flexural strength of beam and column members in RC frame structures. In this way, while permitting calibration of the strength increase in the beam to comply with the strength hierarchy criteria needed for a proper seismic behaviour it can provide additional energy absorption. A numerical evaluation of the SPEAD system is carried out by means of a refined 3D model built with an advanced nonlinear finite element program. The SPEAD system has been virtually applied (through finite element analyses) to an RC external beam-column joint, representative of typical existing RC buildings, and the numerical results are compared to those of a specimen that was not upgraded and subjected to the same experimental tests. The SPEAD upgraded model provided a strength increment of about 50% with also a strong reduction of bond-slip effects in the joint panel region. This latter, in turn, provided a beneficial increase of ductility. Based on the positive results from numerical simulations, a design method is also provided.

1 INTRODUCTION

Recent seismic events in Italy and abroad, (e.g., L'Aquila (Italy) in 2009 [1], Central Italy in 2016 [2], Haiti in 2010 [3], Christchurch (New Zealand) in 2010-2011[4]) have demonstrated the vulnerability of the Italian building inventory, and the need for rapid strengthening of both private and public structures in order to avoid heavy losses in human life and economic repair and reconstruction costs.

As an example, after the 2009 L'Aquila earthquake, a comprehensive repair program of school buildings was carried out by the Province government of L'Aquila, along with the technical collaboration of the ReLUIS network (The Laboratories University Network of Seismic Engineering). By six months from the event on April 6, 2009, many school buildings were repaired and upgraded by means of rapid intervention strategies. As an example, some of these buildings were upgraded by addressing the premature brittle failure of beam-column joints [5].

Significant issues on school buildings were also found in the aftermath of the 2016 Central Italy earthquakes [6]. Many school buildings were unusable, heavily affecting the recovery phase of the local communities.

Thus, cheap and rapid strengthening techniques [7] for repairing and upgrading RC buildings are needed, not only for in the aftermath of a seismic event but, more importantly, in prevention. Indeed, funds used to prevent social and economic losses due to earthquakes are much more effective as they can prevent fatalities, which is priceless.

Under these premises, authors started to develop simple strengthening techniques, focused on RC buildings, for cheap and rapid interventions exploiting previous research from other researchers [8]. They focused their experimental study on a beam-column joint equipped with a system which can increase the seismic performances of RC members, although it requires the demolition and reconstruction of infills in real applications, as well as slab drilling, with associated damage to non-structural components.

In the past, other studies have analysed different strengthening systems. Among them, Kazem Sharbatdar et al. [9] proposed a strengthening technique using curbs to connect beams and columns. They tested two benchmark specimens and two upgraded joints, finding encouraging strength and ductility increases due to the shifted position of plastic hinges in the beam. However, the proposed device requires the demolition of infills and, in the case of internal joints, the curbs reduce the available floor space.

Realfonzo et al. [10] tested eight beam-column specimens, six of which were equipped with FRP systems. They achieved good results in terms of seismic capacity increase, although the strengthening configurations were not easily applicable to real structures due to the presence of the slab and transverse beam, and the requirement for local infill demolitions.

In [11] it is developed a mixed strengthening technique applied to beam-column joints without seismic detailing, conforming to old Indian codes. This was aimed at repairing and strengthening beam-column joints by means of GFRP wraps glued to the beam and column ends, and a steel plate covering the joint region. The major inadequacy of this solution was, as in previous cases, the presence of strengthening devices bonded to regions of the beam-

column specimens where slab and transverse beams are present, preventing application of the intervention to real cases.

Singh et al. [12] experimentally tested a total of nine RC beam-column joints under static loading conditions. The joints were equipped with L-shaped CFRP wraps on the beam and columns, to which 45° wraps were added to strengthen the joint region. This strengthening configuration provided low seismic capacity increases, even though the collapse mechanism became more ductile. However, some difficulties are predictable in real applications to RC frame structures (namely interference with the slab and transverse beam).

In [13], ten scaled reinforced concrete beam-column joints, were cyclically tested under constant axial load. The joints were strengthened with fibre-reinforced polymer (FRP) systems, made up of a combination of carbon and fibreglass fabric, and a hybrid braided FRP fabric. The study demonstrated the proposed technique strongly improves the ductility and dissipation energy of the RC joints, even though demolitions were needed for the installation works. In the study by Wang et al. [14], six beam-column specimens were tested. Four specimens, out of these six were equipped with both externally bonded CFRP sheets and near-surface mounted CFRP strips as strengthening solutions. Results showed that the seismic performance of deficient joints can be significantly improved.

Regarding wide beam-column joints, some researchers [15] developed and numerically analysed a strengthening technique based on CFRP fabrics. This kind of intervention can effectively improve the seismic capacity of beam-column connections and does not need slab drillings, making it less invasive.

The previous examples demonstrate how several materials and configurations may be used to strengthen RC structures through local interventions. Nevertheless, experimental research programs have frequently been carried out on ideal specimens without slabs and transverse beams. Further, in most cases, the abovementioned techniques can encounter substantial difficulties if they require extensive demolition of non-structural components (e.g. infills). This will be reflected in costs and the time needed to carry out interventions, and on social consequences (e.g. moving users to other buildings).

For these reasons, the aim of this study is to develop a strengthening technique for RC frame buildings which is applicable only from outside, without interfering with the slab, transverse beam, and infills, which can easily be installed and is cheap and sustainable. The technique, named SPEAD (Steel Plate Energy Absorption Device), is essentially made up of an opportunely shaped steel plate externally connected to RC beam-column joints by means of glue and bolts. The SPEAD device is able to offer a carefully pre-determined threshold force activated by the beam-column relative deformation, thus increasing seismic capacity and preventing brittle shear failure of the joint region. The system is also able to shift the hinging region of the beam and provide strength increments to the column ends.

In the following, a detailed description of the technique is provided, along with numerical simulations of the system applied to previously tested beam-column joints. Firstly, a detailed nonlinear 3D finite element model is built and calibrated to reproduce the experimental results of the as-built specimens. Afterward, the numerical model is equipped with the SPEAD system to check its effectiveness and seismic capacity improvement. It is worth noting that other researchers utilized numerical simulations to evaluate the effectiveness of strengthening techniques on the local and global behaviour of structures, even in absence of a calibration upon experimental data. As an example, in [16] the behaviour of an RC beam-column joint and a whole two-story plane structure retrofitted with carbon fiber composites was evaluated observing the changes in seismic performances and cracking patterns due to the strengthening intervention. Wang et al. [17] evaluated the effect of prestressed Hybrid Fiber Reinforced Polymers as strengthening intervention for RC beams while in [18] Zhu et al. studied the behaviour of damaged reinforced concrete slab strengthened by means of ultra-high performance concrete.

2 THE STEEL PLATE ENERGY ABSORPTION DEVICE (SPEAD)

Earthquake events have shown some typical damage to RC frame buildings, to beam members (as an example see Figures 1a and b), to columns, or to joint panels. In some cases, combined damage can be also found. Moreover, the low amount of beam reinforcement in under-designed RC buildings (especially for beams not supporting the slab) can lead to beam damage, as reported in Figure 1c, where cyclic lateral loads applied to a beam-column joint caused extensive cracks and consequent low-cycle fatigue failure of rebars [19-20].

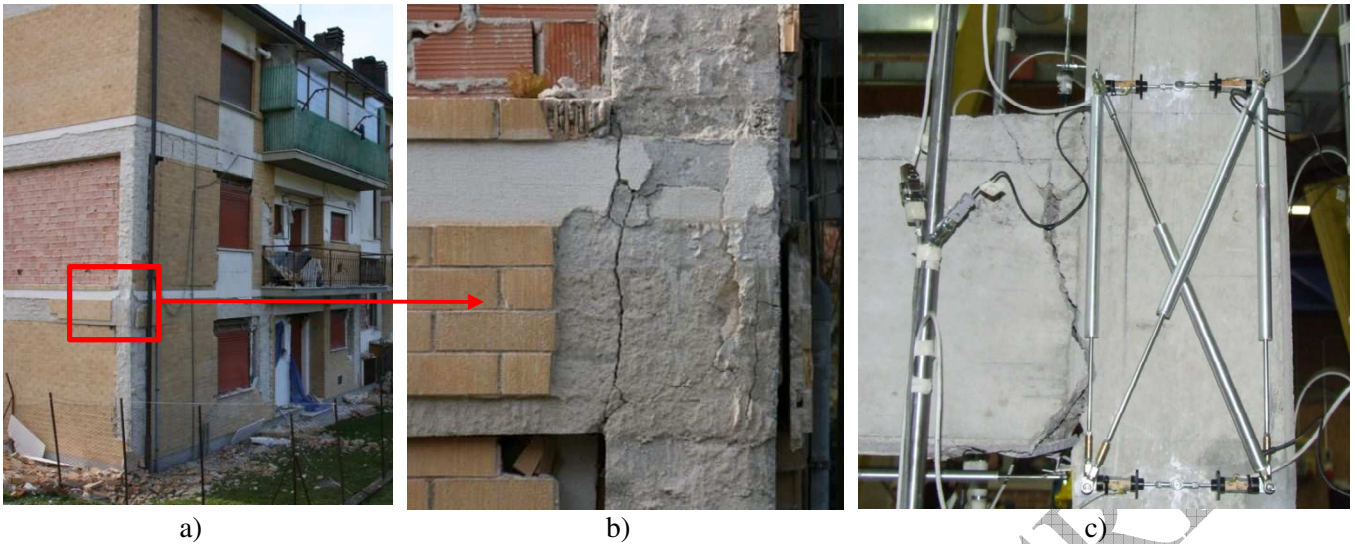


Figure 1. a) Damage to an RC building in Norcia (Central Italy earthquake 2016), b) Detail of a beam-column connection, c) damage to the beam end due to an experimental test on a beam-column joint.

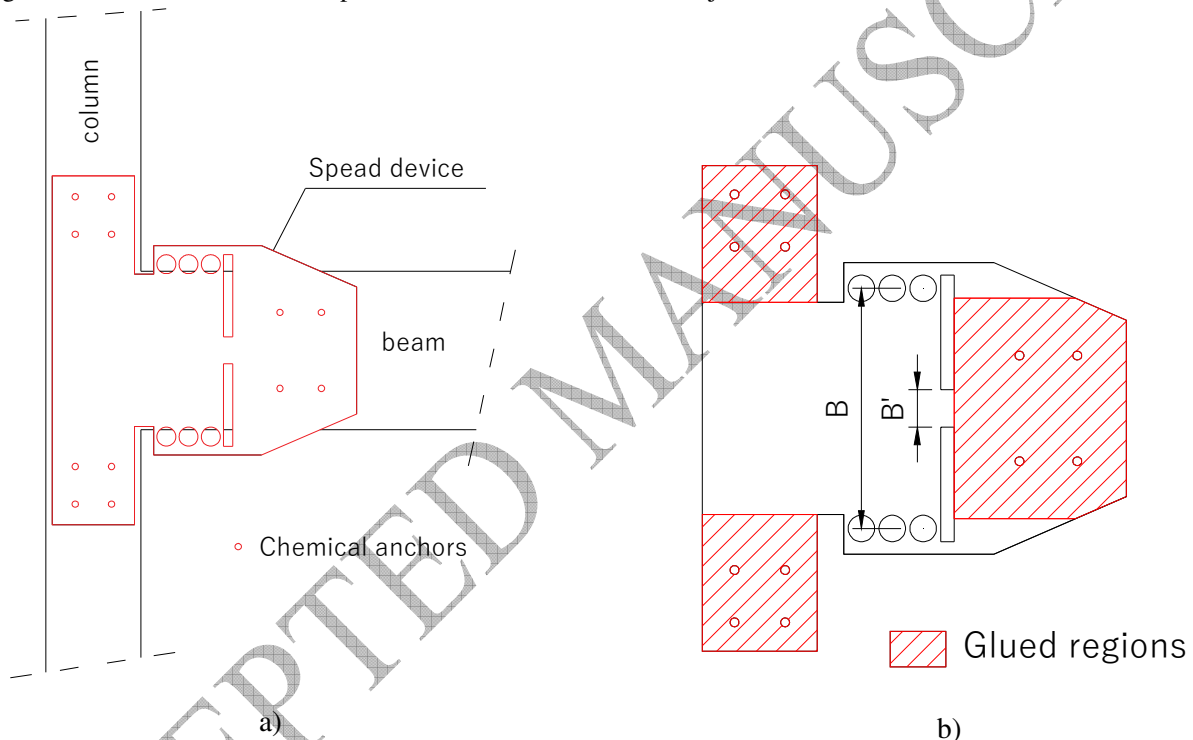


Figure 2. a) SPEAD system applied to a beam-column joint, b) SPEAD device with the glued regions highlighted (red hatch).

In order to increase the strength capacity of the beam-column connections, the SPEAD system (under pending patent submitted to the Italian Ministry of Economic Development - Italian Patent and Trademark Office, with application no.102019000006567) was conceived (Figure 2a). It is a steel plate designed to shift the position of the beam plastic hinge away from the beam-column intersection. It has circular holes, forming hourglasses, that can deform under shear, providing a fixed threshold force and dissipation capacity due to steel hysteresis.

The device is essentially made up of two parts. The first one must be connected to the column and the second one is connected to the beam. The SPEAD system works as a result of the relative deformations between the beam and column. In fact, the borders between the two parts of the device are made in such a way that plastic deformations can easily occur at predefined force thresholds. Figure 3a identifies parts 1 and 2 of the device, highlighted with grey and blue coloured hatches respectively. Figure 3b shows the deformed shape of the device applied to a beam-column connection, while Figure 3c points out forces and moments that one part (say part 2, which is hidden) exerts on the other part once plastic deformations are achieved.

Forces F_P working on the lever arm “B”, moment M_P and shear force V_P developed along the border between part 1 and part 2 of the device contribute to increasing the flexural strength of the beam, whose plastic hinge will develop at the end of the device (on the right of part 2).

It is also worth noting that force V_p allows transferring of a quota of the beam shear directly to the column without requiring a shear upgrading of the beam in the area covered by the device. Moreover, the regions of part 1 in contact with the column add flexure strength due to the steel plate presence. Therefore, when it is necessary to comply with capacity design criteria, these parts can be extended onto the upper and lower column to enhance column strength.

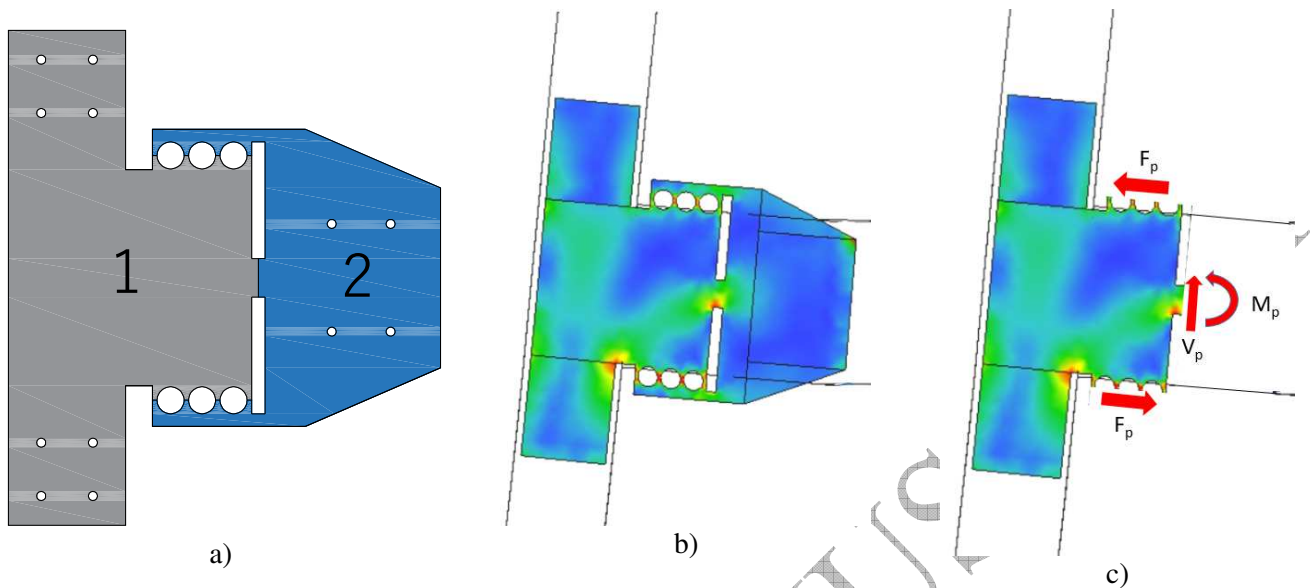


Figure 3. a) Different parts of the SPEAD device, b) deformed device, c) action of part 2 on part 1.

The SPEAD system was conceived to be applied to RC frames from the outside; that is, only on one lateral face of the beam-column connection. Thus, it does not require the demolition of infills, only plaster removal. The SPEAD device is applied through chemical anchors which allow it to be attached to the beam and column members (Figure 3a).

It is important to underline that, in order to improve the connection between the SPEAD and RC members, the SPEAD device is glued to the corner area of both the beam and column members using epoxy resin (Figure 3b). This improves the stiffness of the mutual connections, as well as the bond strength. Degraded concrete regions should be repaired before the application of the SPEAD device in order to obtain a flat surface where the steel plate can be laid. Moreover, to make the connection between SPEAD and the concrete members stronger and reduce problems related to possible concrete spalling under high seismic actions, additional chemical anchors have to be installed as displayed in Figure 2.

As can be seen in Figure 2, there is no connection between the SPEAD and the joint panel region. This is a desirable feature to avoid additional shear stresses acting in that area. Indeed, the additional flexure capacity of the upgraded beam is transferred directly to the column end, and not through the joint core.

Most of the flexural response of the SPEAD is determined by the internal lever arm “B” (Figure 2b), where the centroid of the hourglass forces F_p is placed. Another source of flexural strength is provided by the rectangle between the two rectangular holes. This also provides shear strength, allowing the hourglasses to work in the right way.

The relative deformation between the beam and column can yield the hourglasses (mainly under shear) and the rectangle in order to generate a certain additional flexural strength of the beam, whose values should be determined by means of the design method proposed later.

It is important to underline that, even though the device is applied only on one side of the beam, the presence of the RC slab on the other side is able to provide the needed counterbalance in terms of strength and stiffness thus preventing possible eccentricity.

The system is thought to provide additional strength in a beam-column connection by increasing the beam flexural bending value, while maintaining the capacity design principles. Therefore, the system is more appropriate for a beam-column connection in which the beam member is not much stronger than the column. The typical case is a beam-column joint where the beam is not supporting slab, and for this reason has a small amount of steel and is weaker than the adjacent column. However, for each specific case, to fully comply with capacity design principles the designer has to evaluate the possible need to strengthen the upper and lower columns through other techniques eventually combined with the presence of the SPEAD parts applied to the column. Moreover, it is useful to remind that the new location of beam the plastic hinge could not have an appropriate detailing devoted to avoid rebars' buckling and provide concrete confinement. For this reason, in the design process, the possibility of a local

strengthening (e.g. through unidirectional FRP composites) in the new plastic hinge location of the beam should be attentively considered according to the details of the considered beam-column joint.

2.1 Design Method

In order to describe the proposed design method, a simple model of a beam-column joint is shown in Figure 4 according to two different conditions: the first (Figure 4a) is related to the as-built condition, where the beam (whose depth is h_b) plastic hinges (point E) begin at the interface with the column (having depth equal to h_b). The blue segments refer to rigid offsets where no yielding is allowed. The second (Figure 4b) is related to the upgraded situation, where the first plastic hinge forms at the end of the SPEAD device (point B) and a second one forms, possibly simultaneously, at point A—that is, the centre of the SPEAD system (able to absorb energy under cyclic loading). For the purpose of the design method, the parts covered by the SPEAD device are assumed to not be subjected to yielding (blue segments in Fig. 4b, whose dimensions are d over the column and c along the beam). As already said, it is worth specifying that, in real cases, the eccentricity caused by the SPEAD device (which is attached to only one side of the beam) is absorbed by the slab on the other side of the beam. Due to this, the adopted plane models (see Figure 4) permit to effectively analyse the upgraded specimen.

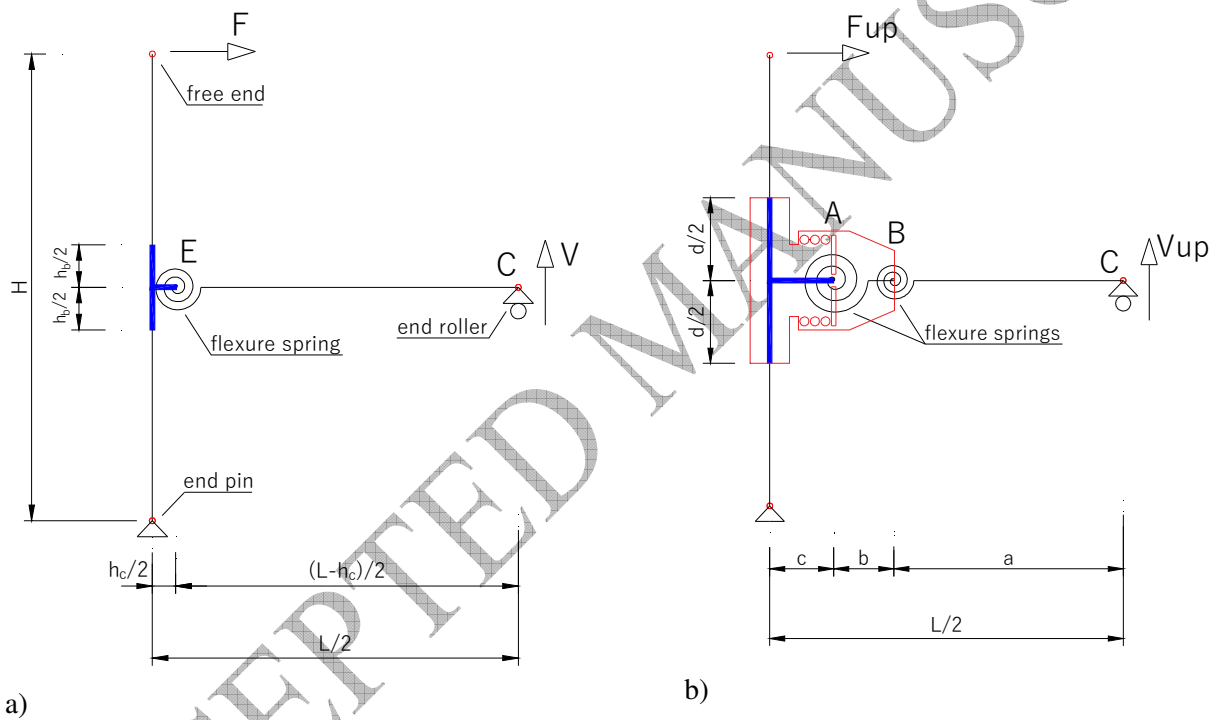


Figure 4. Loading schemes in the as-built (a) and upgraded (b) conditions.

In the as-built condition, the capacity F of the beam-column specimen is derived from equilibrium, as follows:

$$F = \frac{VL}{2H} \tag{1}$$

where L is the total beam length, H is the total length of the top and bottom columns, and V is the beam shear strength due to vertical reaction at C . This latter can be also obtained from:

$$V = \frac{2M_{yE}}{L-h_c} \tag{2}$$

where M_{yE} is the yielding moment at the point E and h_c is the column depth.

In the upgraded condition, one must have:

$$F_{up} H = V_{up} \frac{L}{2} \tag{3}$$

where F_{up} is the capacity of the beam-column specimen after strengthening while V_{up} is the beam shear strength due to vertical reaction at support C . This latter can be also obtained from:

$$V_{up} = \frac{M_{yB}}{a} \tag{4}$$

where M_{yB} is the yielding moment at the point B and a is the beam length measured from support C to B . As a consequence, Eq. 5 can be written as follows:

$$F_{up} = V_{up} \frac{L}{2H} = \frac{M_{yB}}{a} \frac{L}{2H} \quad (5)$$

The upgrading factor U can be derived as follows:

$$U = \frac{F_{up}}{F} = \frac{M_{yB}}{M_{yE}} \frac{L-h_c}{2a} \quad (6)$$

representing the upgrading factor obtained only by shifting the plastic hinge from the joint.

In order to obtain the simultaneous yielding in A, it must be:

$$M_{yA} = V_{up} (a + b) = \frac{M_{yB}}{a} (a + b) \quad (7)$$

with V_{up} derived from Equation (4), M_{yA} is the yielding moment in A and b is the distance between the centre of the SPEAD device (A) and the point B. M_{yA} is the sum of the contributions of the RC section (M_{yAC}) and the SPEAD system (M_{ySP}), that is:

$$M_{yA} = M_{yAC} + M_{ySP} \quad (8)$$

In this way, one can design the bending moment of the SPEAD device, as follows:

$$M_{ySP} = \frac{M_{yB}}{a} (a + b) - M_{yAC} = M_{yB} \left(\frac{a+b}{a} - 1 \right) \quad (9)$$

where M_{yB} has been assumed equal to M_{yAC} .

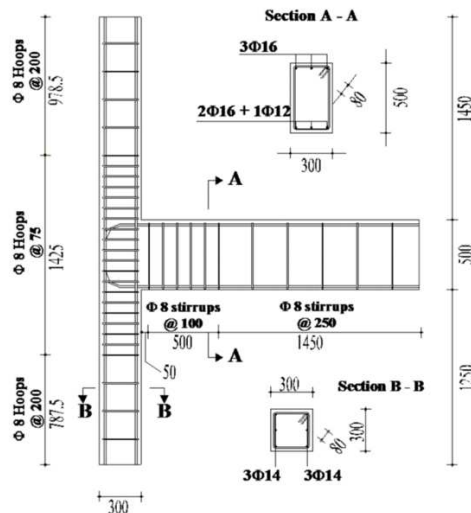
The proposed system can be applied only if the shear failure of segment B-C of the beam can be excluded in the as-built condition, or after a shear strengthening intervention. It also has to take into account that the column end framing in the joints are covered by the SPEAD device, thus offering additional flexural and shear resistance. This condition must be carefully considered to verify that the capacity design is guaranteed after the SPEAD application.

3 ANALYSES OF THE AS-BUILT SPECIMEN

The proposed system has been numerically tested on a beam-column joint specimen previously designed and analysed in the framework of a wide experimental program and presented in detail in [19-20]. The experimental results are briefly described in the following section, along with the Finite Element (FE) modelling performed in order to reproduce the observed behaviour of the specimen. This latter step of the study is fundamental to check the effectiveness of the adopted FE modelling in predicting the expected behaviour of the upgraded specimen; that is, the specimen equipped with the SPEAD device.

3.1 Experimental Results and Numerical Simulations

The considered external beam-column (BC) joint (named T5) was assumed to belong to a transverse frame of an RC 4-storey residential building with a constant inter-storey height of 3.2 m. The beam is not supporting the slab, whose joists are parallel to it. It has been designed according to the past seismic code [21] as belonging to a low ductility class (CD" B") frame placed in seismic zone 2 with $a_g = 0.25$ g, where a_g is the design ground acceleration at the ultimate limit state on type A ground [22]. During the experimental tests, the specimen was subjected to a normalised axial load equal to $v=0.15$, corresponding to a force value of $N=290$ kN. The geometry of the joint specimens is shown in Figure 5. The choice of this specimen was due to the fact that it was the only one subjected to joint panel cracking in addition to flexure cracking to the beam, near the column interface. Under these conditions, it was interesting to explore the effectiveness of the proposed device in protecting the joint panel from damage.



a)

Figure 5. Geometry and detailing of joint specimen T5.

At the time of experimental testing, some of the cubes prepared during the concrete casting were subjected to compression tests in order to estimate their strength, achieving a mean cylinder value equal to $f_c=21.5$ MPa. Based on this value, all other characteristics of the concrete (e.g. tensile strength) were derived for finite element modelling, as described in the following section.

The reinforcement bars are of class B450C according Italian structural code [23] and corresponding to hot rolled steel of class C according to the Eurocode 2 [24]. Tensile tests undertaken on the steel rebars for each bar diameter showed they could assume a mean yielding stress of 480 MPa and failure stress of 590 MPa at a strain of 12%.

The experimental loading scheme was such that a horizontal load (displacement controlled) was applied to the top of the column with a pin restraint at the down end of the column, while a pin roller was applied to the beam end.

The complete loading scheme and history are reported in the aforementioned paper by Masi et al. [20]

Finite element modelling of the specimen was carried out using the software package ATENA 3D version 5.4.1 [25] through hexahedral linear (4-noded) finite elements for concrete members. Reinforcing bars were modelled by truss elements embedded in concrete (Figure 6) capable of absorbing axial loads only. In total, the finite element model is made of 1363 truss elements, 2112 tetrahedral elements, and 2645 hexahedral elements, with 5844 nodes globally.

The mean size of the hexahedral elements was 0.06 m, obtained through a sensitivity analysis.

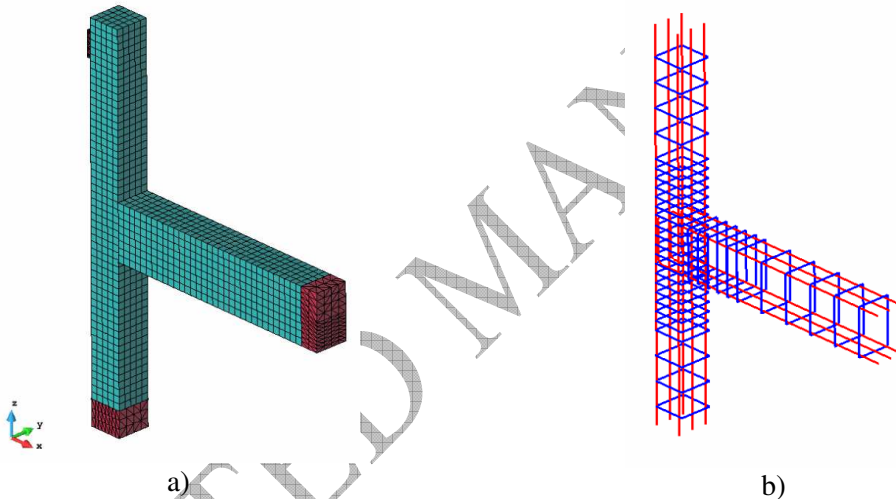


Figure 6. 3D finite element model **a)** volume mesh with brick and tetra elements, **b)** truss elements modelling the reinforcement cage of specimen T5.

The details required for explaining the nonlinear model simulating the behaviour of reinforced concrete structures are reported here. For additional information, the reader can refer to the ATENA program documentation [22].

The formulation of constitutive relations was considered in the plane stress state. A smeared cracks approach was used to model the damage. The nonlinear behaviour of concrete in the biaxial stress state is described by means of the effective stress σ_c^{ef} and the equivalent uniaxial strain ϵ_{eq} . The equivalent uniaxial strain was introduced in order to eliminate the Poisson's effect in the plane stress state. The complete equivalent uniaxial law for concrete is depicted in Figure 7a.

The behaviour of concrete under tension is linear until the tensile strength f_t^{ef} is achieved. Once the tensile strength is reached, a fictitious crack model based on a crack-opening law and fracture energy is used for modelling crack propagation in concrete. Among several crack opening laws available in ATENA, the exponential one was selected [26], as can be seen from Figure 7b.

The compressive strength f_c^{ef} is assumed as the mean value obtained from the compressive tests on cubes mentioned earlier. This latter is $f_c^{ef}=21.5$ MPa. From the same compressive test on cubes, it was possible to determine the characteristic compressive strength, that is $f_{ck}=17.3$ MPa.

According to the characteristic compressive strength, the tensile strength was determined based on the expression provided in Eurocode 2 [24], that is:

$$f_t^{ef} = f_t = 0.3(f_{ck})^{(2/3)} = 2.0 \text{ MPa}$$

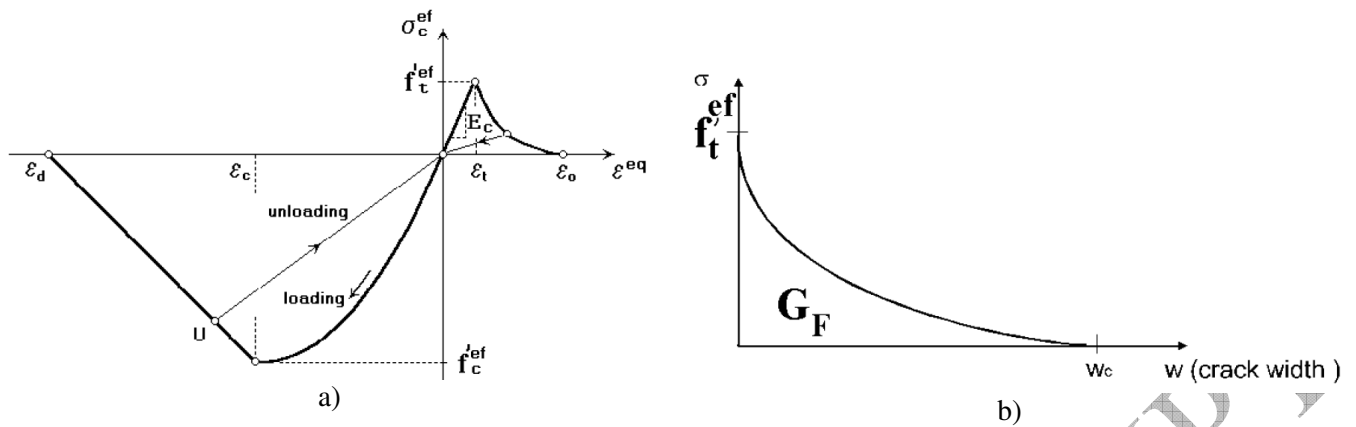


Figure 7. Complete uniaxial stress-strain law **a)** and exponential crack opening law in tension **b)** for concrete.

In the smeared cracking approach, a significant role for the accuracy of the model is played by the value of the fracture energy G_F , which was evaluated, in absence of direct experimental data on the used concrete, by means of the expression reported in Model Code [27-28]:

$$G_F = G_{F0} \cdot (f_{cm} / f_{cm0})^{0.7} = 0.181 \text{ N/mm}$$

Where $f_{cm0}=10\text{MPa}$ and $G_{F0}=0.106\text{N/mm}$ for concrete with crushed basalt aggregate, as in this case. Table 1 summarises the parameters selected for the adopted concrete model, named in the framework as *CC3DNonLinCimentitious2*.

Table 1. *CC3DNonLinCimentitious2* concrete model parameters.

Parameter	Units	Value
Uniaxial compressive strength f'_c	(MPa)	-21.00
Elastic modulus E_c (MPa)	(MPa)	32500.00
Strain at compressive strength	[-]	-0.002
Tensile strength f_t (MPa)	(MPa)	2.00
Unit fracture energy (N/mm)	N/mm	0.181

A hardening multilinear behaviour was considered for the steel reinforcement. The steel elastic modulus was set equal to 200.000 MPa and the yielding stress was $f_y = 480$ MPa according to the experimental results obtained from tensile tests on steel specimens, as stated previously. The same constitutive law is assumed for both longitudinal and transverse reinforcement.

ATENA 3D can simulate the bond between concrete and steel by means of nonlinear springs [29] whose constitutive laws have to be carefully evaluated. In this study, the CEB-FIP model code [27-28] bond law was used. Making this assumption and considering that ribbed bars are present, the peak bond stress is $\tau_{max} = 2 \cdot \sqrt{f'_c} = 9.27\text{MPa}$ while the residual value is 15% of the peak: $\tau_f = 1.39\text{MPa}$ with $s_1=s_2=0.6$ mm and $s_3=2.5$ mm (see Figure 8).

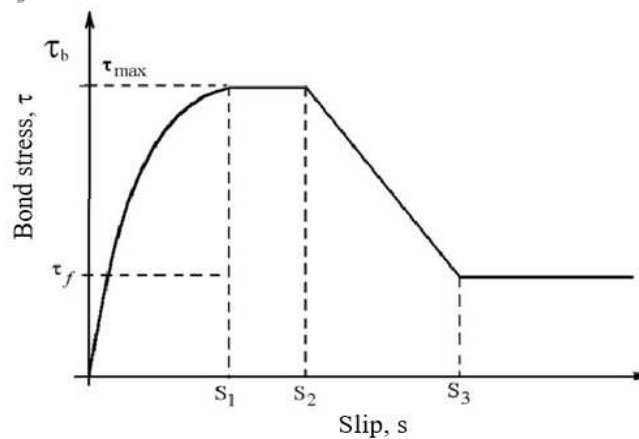


Figure 8. Bond model (CEB-Fip model code).

The numerical analyses were displacement controlled by applying a horizontal displacement at the top of the column in a monotonic way. When performing the monotonic analyses, two separate simulations were necessary to apply positive and negative displacements to the column.

3.2 Comparison Between Experimental and Numerical Results

Experimental results related to the as-built specimen have already been published [19-20] as part of a comprehensive research program. For this type of joint specimen, a mixed failure mechanism was observed. In fact, the degrading phenomena are characterised by both flexural damage to the beam and diagonal cracking in the joint panel. Moreover, the sub-vertical crack in the beam near the intersection with the column occurred before the first diagonal crack appeared in the joint panel.

During the test, the first vertical crack in the beam was clearly observed when the top displacement was equal to 45 mm, corresponding to a drift value of 1.4%. At that stage, no cracks in the joint panel were visible. Small diagonal cracks (smaller than half a millimeter) were visible when the applied displacement was equal to 75 mm, corresponding to a drift of 2.3%.

By means of the above numerical model, it was possible to predict the crack patterns and their width. Figure 9 displays the comparison between the experimental and the numerical crack patterns in the two abovementioned fundamental stages of the damage process. As can be seen, a significant correspondence is found with the crack patterns being so similar in the both shape and width.

This latter finding clearly demonstrates that the priority of degrading phenomena affecting the behaviour of the joint specimen is carefully predicted by the numerical simulation with the ATENA software package.

Similarly, to the damage patterns, the global response of the numerical model is important to evaluate how good the calibration of the governing parameters is, especially those related to the concrete behaviour; for example, the compressive and tensile strength of the concrete, as well as the fracture energy and concrete-steel bond behaviour.

This is the reason why comparing the global load-displacement curves obtained from the experimental test and the numerical analysis is of fundamental importance.

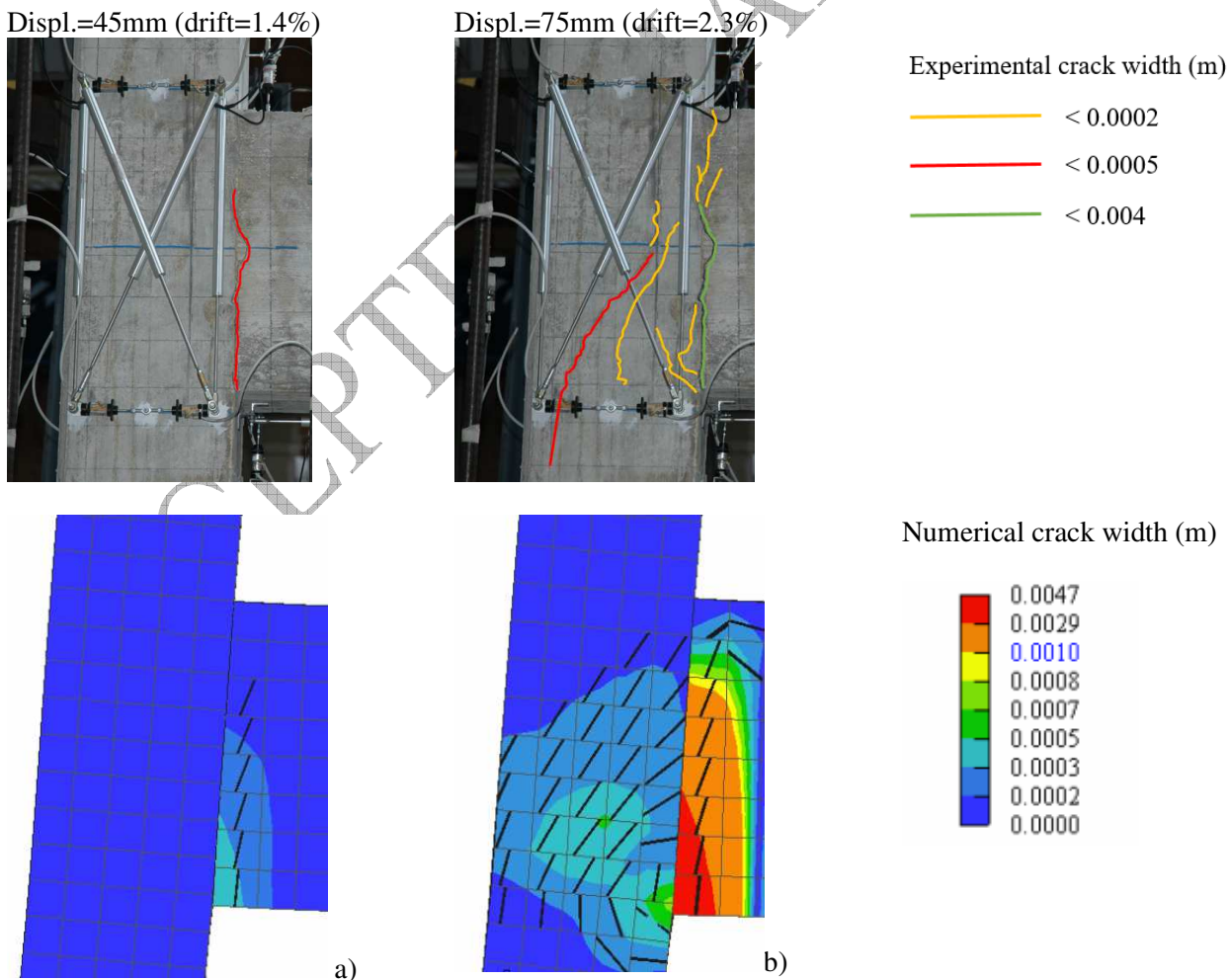


Figure 9. Experimental versus numerical crack patterns at the occurrence of the **a)** cracking in the beam and **b)** in the joint panel.

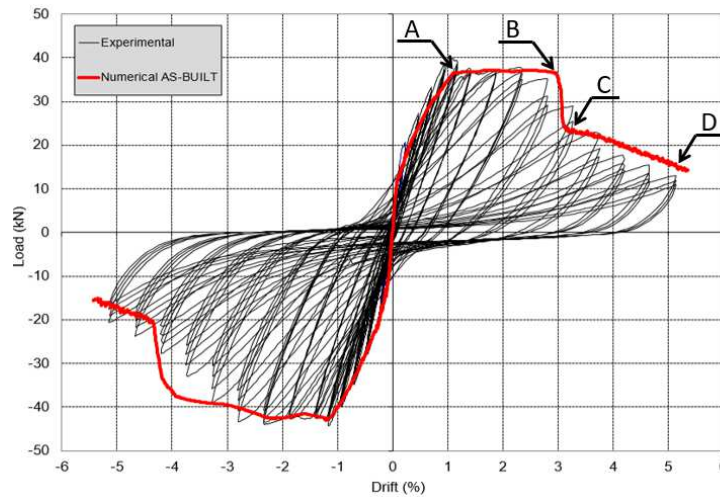


Figure 10. Experimental load-drift cycles envelope versus numerical monotonic load-drift curve.

As can be seen from Figure 10, the numerical load-drift curve (red bold line) obtained by means of the finite element model fits the envelope of the experimental cycles well at different drift amplitudes. In particular, the numerical model is capable of reproducing localised strength drops in terms of the drift at which it occurs and their magnitude. Numerical results are reported in detail in Table 2. Peak forces for both negative and positive loading are predicted with a small scatter compared to the experimental ones. Larger scatter (still acceptable) is found on the estimation of the ultimate drift, where an overestimation of about 13% is found. This reflects on the prediction of the displacement ductility. However, good agreement between the experimental and numerical results is confirmed.

Table 2. Comparison between experimental results and numerical simulation.

Performance Parameter	Experimental	Numerical	Δ (%)
F_{max} (kN)	39.03	36.5	-7.12
F_{min} (kN)	-44.20	-42.9	-2.94
d_{u+} (%)	3.25	3.00	-7.69
d_{u-} (%)	-3.60	-4.10	13.89
d_{y+} (%)	1.00	1.13	13.00
d_{y-} (%)	-1.15	-1.17	1.74
μ_+ (-)	3.25	2.65	-18.31
μ_- (-)	3.13	3.50	11.94

In order to explain localised strength drops, critical points of the load-drift behaviour have been highlighted in Figure 11, labelled with the letters A (yielding), B (end of the plateau), C (end of the localised strength drop), and D (maximum drift).

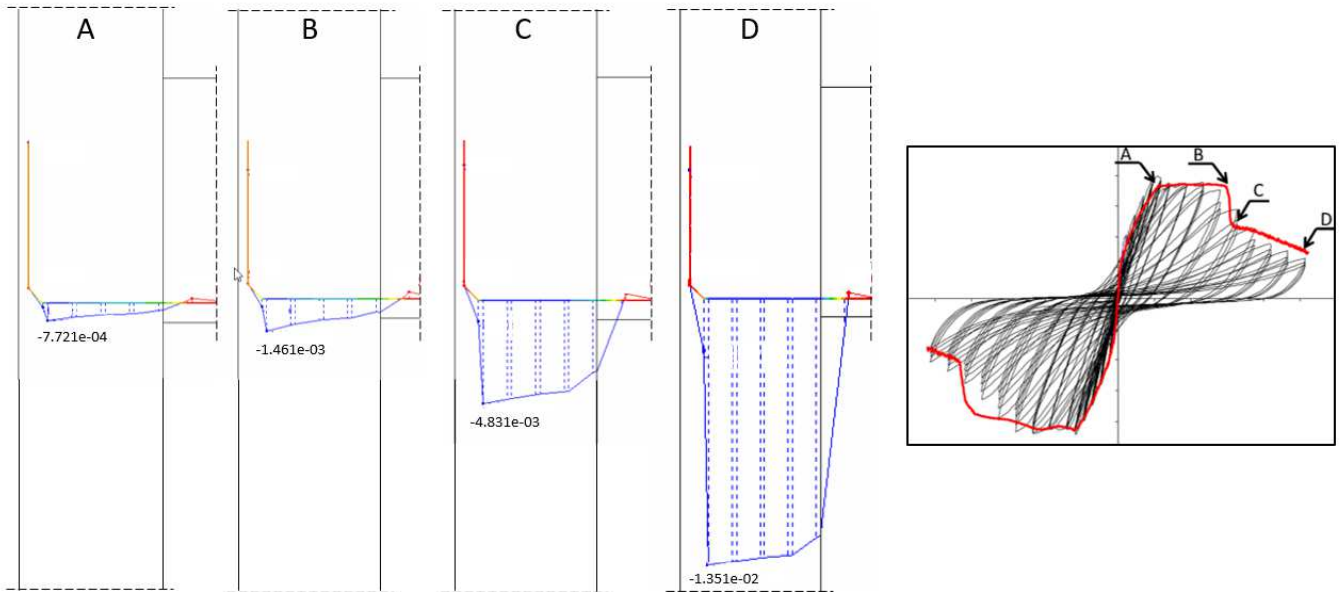


Figure 11. Evolution of the bond slip of the external bottom beam bars (16 mm diameter) for positive loading (slips in (m)).

At those critical points, the bond slip affecting the external beam rebars is also depicted in Figure 11, where the outline of the beam-column intersection is reported, along with the profile of the bottom bars of the beam with the bond slip evolution along its length. This latter finding is related to one external bar and can be assumed as representative of the other bottom bars. As can be seen, at point C the slip is more than three times that of point B, and this causes a stress drop in the beam bars responsible for the sudden load decrease.

4 ANALYSES OF THE UPGRADED SPECIMEN

In this section, the SPEAD system is applied to the specimen described above in order to verify its effectiveness in upgrading seismic performance. For this purpose, numerical analyses have been carried out by using an FE model performed in the ATENA framework, which is, as reported above, able to reproduce the expected behaviour of the specimen. FE modelling has been firstly adopted to design the proposed strengthening device and then to perform a comparison between the as-built and upgraded specimens.

4.1 Finite Element Analysis of the SPEAD System

Starting from the dimensions of the specimen under study (i.e. $a=1.52$ m; $b=0.4$ m; $L=4.7$ m; $hc=0.3$ m, see Fig. 4), Equation 9 allows us to calculate the resisting moment to be provided by the SPEAD system; that is:

$$M_{ySP} = 0.26 M_{yB} = 28.6 \text{ kNm},$$

where is $M_{yB} = 110 \text{ kNm}$ for joint T5. The upgrading factor (Equation 6) is $U=1.44$.

FE analyses have been carried out in order to calibrate the SPEAD dimensions, so it is able to provide the above-reported value of M_{ySP} (i.e. 28.6 kNm). In fact, the bending moment provided by the SPEAD requires certain dimensions for the device, especially concerning the plate thickness, dimensions of the rectangular (and consequently B') and circular holes, and the internal lever arm B . In particular, most of the resisting bending moments around the pole P (Figure 12) is provided by the shear forces needed to deform the hourglasses, which have an internal lever arm equal to B ; a quota of the flexural strength is provided by the rectangle of dimension B' , whose main purpose is to resist shear to avoid tensile stresses on the hourglasses. For design purposes, some of the above parameters can be preliminarily assumed (e.g. plate thickness, dimensions of both the rectangular and circular holes), while an iterative procedure performed by gradually increasing dimension B can be adopted to evaluate M_{ySP} .

In this case, the circular hole diameters are assumed to be equal to 60 mm, the thickness is 10 mm, and $B'=85$ mm. The number of holes is chosen in order to have a number of hourglasses sufficient to guarantee stable hysteretic behaviour if one of them fails under seismic loading. In this case, three holes provide four hourglasses. The hole diameters determine the minimum thicknesses of single hourglasses. This, in turn, influences the shear force needed to plastically deform it, obtaining the wanted value F_P . In this case, the minimum hourglass thickness is $t_h=10$ mm.

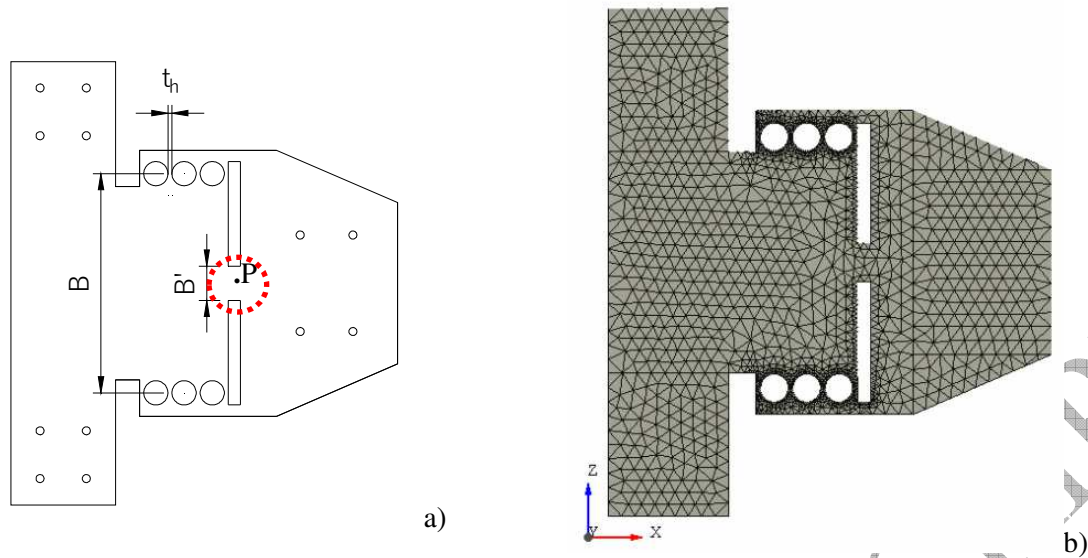


Figure 12. Geometric model of SPEAD device **a)** and FE model **b)**.

Finally, dimension B' has to be large enough to provide a shear stiffness to the connection between parts 1 and 2 in order to avoid excessive tensile stresses in the hourglasses, which must work essentially under shear.

A plate thickness equal to 10 mm has been determined to avoid buckling of device regions working under compression. However, this problem can also be solved by using stiffening ribs welded orthogonally to the plate. Details about this aspect are beyond the scope of this study. Therefore, numerical simulations described in the following do not consider out-of-plane degrees of freedom of the plate.

An FE model with 2D elements has been built with ATENA software [25], which has been fully restrained at the regions in contact with the column and loaded by a prescribed displacement in the region in contact with the beam. The model is made of 3029 triangular linear elements whose dimensions are in the range of 5–30 mm. As can be seen from Figure 12b, a finer mesh is adopted where more plastic deformation is expected, such as near to the hourglasses and next to the rectangular holes.

The material is a steel of class S355 according to the Italian seismic code [23], having a characteristic yielding stress value equal to $f_{yk} = 355$ MPa. The constitutive model is elastic-perfectly-plastic, with a hardening modulus of 1000 MPa.

By means of several analyses, each one corresponding to a different FE model, the optimum value of B has been determined to be equal to 540 mm. In fact, once diameter and hourglass thickness are defined, the yielding force F_p is known. Therefore, by varying the lever arm B , one can modify the flexural response of the device: M_{ySP} .

Figure 13 shows the deformed shape of the device at first yielding (i.e. when Von Mises stresses achieve 355 MPa). As can be seen, the areas that yield first are the hourglasses, according to the desired behaviour. The distortion of the device corresponds to a drift value of about 0.7%, which is next to the yielding drift of the beam-column specimen in the as-built condition. Measuring the bending moment around the Y -axis normal to the plane of the device and passing from the pole P (see Figure 12b), one can obtain a value of 28.1 kNm—very close to the $M_{ySP} = 28.6$ kNm required when applying the designed method.

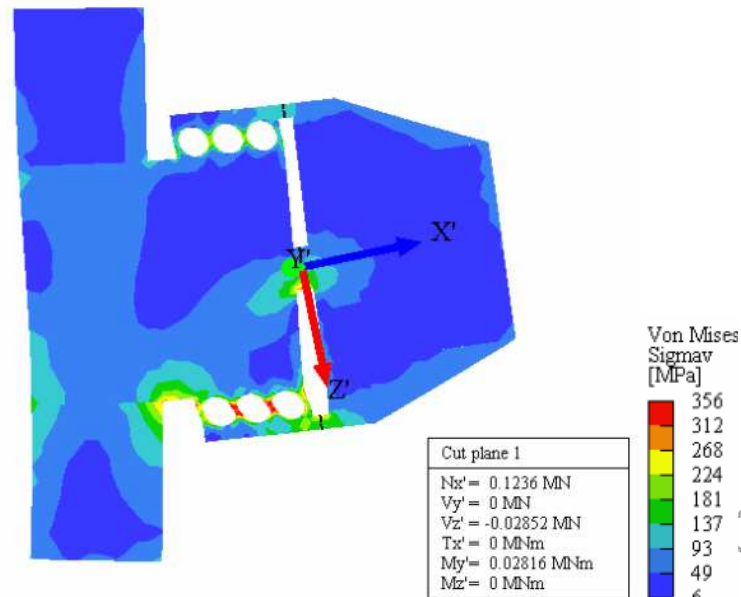


Figure 13. Deformed shape of the SPEAD at yielding and Von Mises stress values.

4.2 Comparison Between As-Built and Upgraded Specimens

In order to check the effectiveness of the SPEAD device in improving the seismic performance of beam-column joints, FE modelling for the upgraded condition has been set up (Figure 14). Assumptions about material properties, restraints, and loading condition are the same as for the individual model of the BC connection (see Section 3.2) and of the SPEAD device (see Section 4.1). In order to simulate the real installation modalities mentioned earlier (i.e. bolts and epoxy resin in selected regions of the contact between the RC joint and the SPEAD device), perfect constraints have been assumed in the contact regions between the two elements.

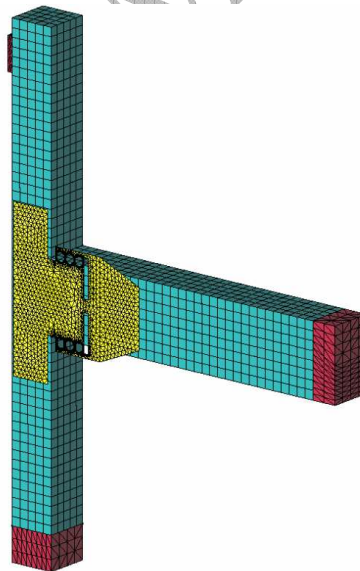


Figure 14. FE model equipped with the SPEAD device.

The model was subjected to a monotonic simulation like the as-built specimen (see Section 3.3), in order to find the differences in terms of seismic behaviour.

Figure 15 and Table 3 show the analytical comparison between the as-built model and the one that has been upgraded with the SPEAD system.

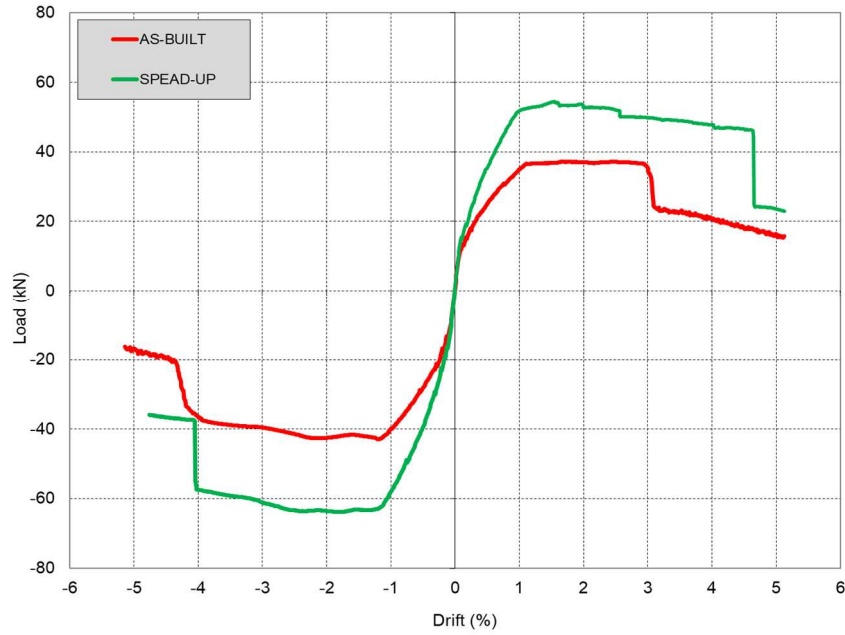


Figure 15. Numerical load-drift curves of the as-built specimen and the SPEAD upgraded model.

Table 3. Performance comparison between the as-built and the upgraded specimen models.

Performance Parameter	AS-BUILT	SPEAD	Δ (%)
F_{max} (kN)	36.5	54.40	+49.0
F_{min} (kN)	-42.9	-63.81	+48.0
d_{u+} (%)	3.00	4.60	+53.0
d_{u-} (%)	-4.10	-4.10	0.00
d_{y+} (%)	1.13	0.99	-13.00
d_{y-} (%)	-1.17	-1.15	-2.00
μ_+ (-)	2.65	4.64	+75.00
μ_- (-)	3.50	3.56	+1.00
K_{sec} ($d=0.33\%$)	1.94	2.63	35.0
K_{sec} ($d=0.50\%$)	1.60	2.30	43.0

The behaviour of the upgraded specimen is better in terms of both strength and stiffness. The initial stiffness is clearly higher for the upgraded model, as yielding occurs at almost the same drift value of 1.0% with different load values, equal to 52 kN and 36 kN respectively for the SPEAD and the as-built specimen (positive loading). This means that about 44% of the stiffness increment has been obtained through the strengthening intervention. Evaluating the secant stiffness at early stages of the load-drift curve, slightly different values are found. At 0.33% drift (corresponding to the occupancy limit state according to the Italian building code), the SPEAD model is 35% stiffer than the as-built model while at 0.5% drift (damage limit state) a 43% difference is found. These stiffness increments due to the SPEAD device suggest further investigation on its effects on a whole structure and not only on a single beam-column joint.

The maximum (F_{max}) and minimum (F_{min}) loads are subjected to an increase (Δ) of about 50%, slightly higher than the upgrading factor evaluated through Equation 6 $U=1.44$. This difference can be ascribed to the steel hardening effect.

It is important to underline that ductility in the positive loading direction increases by 75%, while in the negative direction it remains almost unchanged. This can be explained by the fact that the load drop of the as-built specimen in the positive loading direction was mainly caused by slippage phenomena occurring to the bottom beam rebars. In the SPEAD model, as the beam plastic hinge is shifted away from the joint core, the rebars are not affected anymore by bond-slip.

The sudden load drops occurring to the SPEAD model are related to the tensile failure of one beam rebar due to excessive strain.

Due to computational constraints it was not possible to perform cyclic analyses. For this reason, the dissipation capacities in the upgraded condition could not be fully evaluated, although the monotonic behaviour is somehow representative of the added energy absorption provided by the SPEAD system, through the increased strength and ductility performances. On the other hand, the choice of making monotonic analyses is corroborated by the fact that they have already shown to be effective in the interpretation and understanding of experimental results from tests under cyclic loads [e.g. 30-32].

In order to give evidence of the effects of the SPEAD system on the beam-column joint behaviour, the bond-slips of one of the beam bottom rebars have been plotted for both the as-built specimen and the SPEAD upgraded specimen. As can be seen from Figure 16, the peak value of the total bond-slip is higher for the as-built specimen due to the reduced bond length, which is practically equal to the column depth. The SPEAD specimen shows bond slips equal to about 2.6 and 3.5 times lower than the as-built specimen, respectively, at the peak load and at 3% drift value. This latter finding is due to the larger bond length of the SPEAD specimen, in which the beam plastic hinge is shifted away from the column interface.

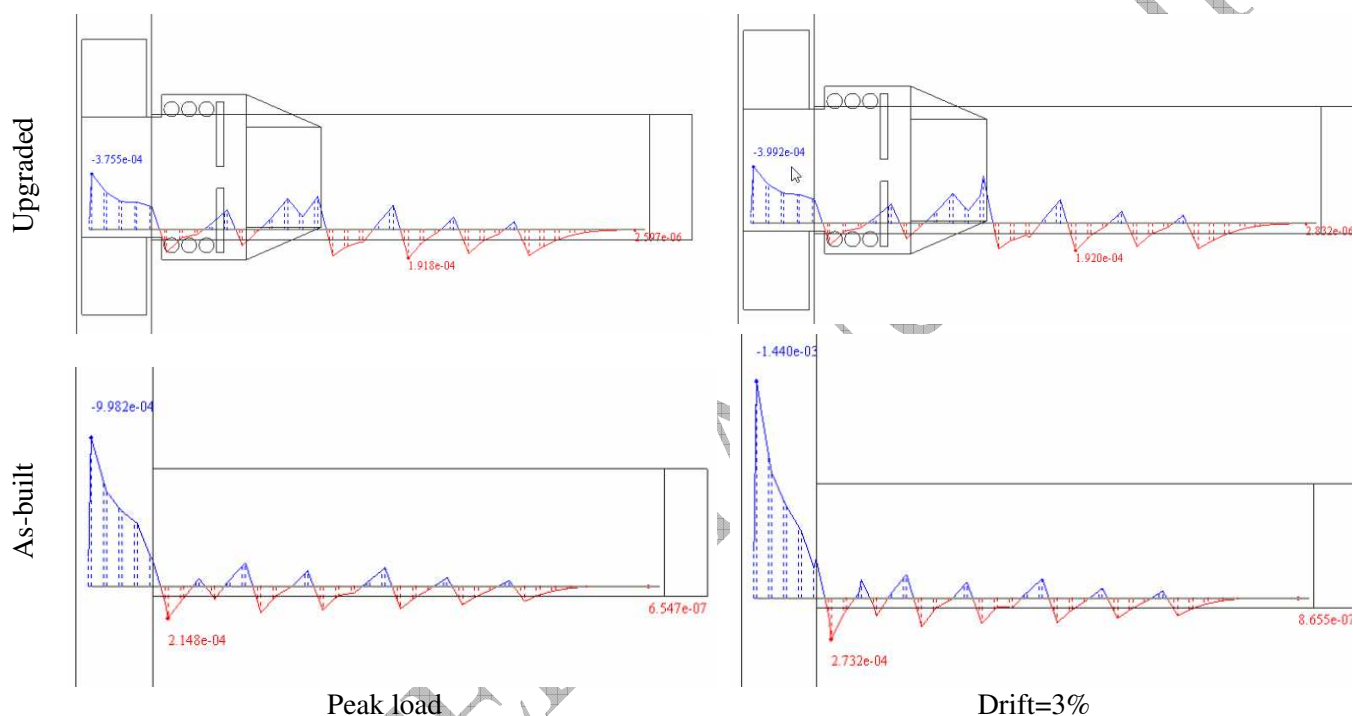


Figure 16. Comparison of bond slip evolution in bottom beam rebars at peak load and at 3% drift value.

It is also interesting to check for the effects of the SPEAD system on reinforced concrete members. An effective way to do this is to plot the cracking patterns of the as-built specimen and those of the upgraded one.

Figure 17 reports the cracking pattern, along with the estimated crack width, in correspondence with a load value equal to $F=36.5$ kN—that is, the peak load of the as-built condition. As can be seen, the upgraded specimen is far from yielding, and the cracks have a thickness lower than 0.44 mm at the region where the SPEAD device ends. The as-built model shows a cracking pattern spread into the joint panel, with a crack width of 0.5 mm and much higher at beam-column intersection (cyan colour areas have crack widths out of the scale). The joint panel in the upgraded condition is almost undamaged, showing few cracks of negligible width.

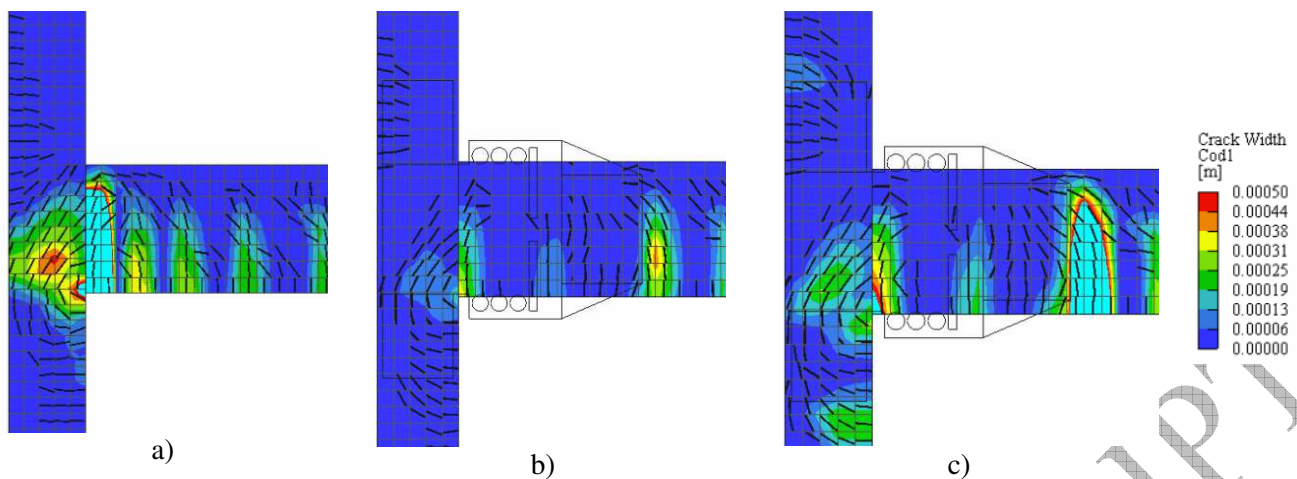


Figure 17. Crack patterns of the as-built and SPEAD strengthened specimens at the peak load of the as-built specimen (36.5 kN).

Figure 17c show the crack width of the SPEAD model at its peak load (54 kN) for positive loading. Most of the damage occurs at the end of the SPEAD device, where the beam plastic hinge is located. The joint panel shows cracks with a maximum width of about 0.25 mm; half that compared to the case of the as-built condition (0.5 mm). This demonstrates the ability of the SPEAD device to limit shear stresses in the joint area, avoiding criticisms that arise when the damage affects the joint region.

CONCLUDING REMARKS

This study aimed to a numerical assessment of a new strengthening technique for RC frame buildings, applicable from the outside, without interfering with the slab, transverse beam and infills, easy to install, and therefore cheap and rapid. The SPEAD system (Steel Plate Energy Absorption Device) increases the beam resisting moment, maintaining capacity design principles between the beam and column.

Simple design indications were used to predict the additional resisting bending moment that the SPEAD device needed to provide in order to obtain a preassigned capacity for the whole beam-column connection. Following this, nonlinear analyses of the SPEAD were performed to detail the device in terms of dimensions and shape.

After building and calibrating a nonlinear FE model of an RC beam-column joint previously tested under cyclic loads, the SPEAD device was introduced to verify the behaviour of the specimen in the presence of the upgrading intervention. The effect of the SPEAD device is very favourable because it is able to increase the strength and ductility of the beam-column connection, as foreseen through the design method. Beneficial effects have also been observed in terms of the damage pattern. In fact, lower damage can be found in the joint panel of the upgraded specimen model with respect to the as-built condition. The additional bending moment of the beam is transferred to the column through the SPEAD device, and not across the joint panel. Other beneficial effects are related to lower bond slip phenomena due to the shifted position of the beam plastic hinge. Due to this, the bond demand of the beam rebars is not concentrated in the joint panel but distributed in a wider beam region between the beam-column interface and the end of the SPEAD device.

For these reasons, the SPEAD device can be proposed as a sustainable strengthening technique, used alone or in combination with other local or global upgrading techniques. Further study is needed to experimentally verify the reported findings, and to quantify the effects of SPEAD devices on whole RC structures through case studies. This latter aspect will be checked by nonlinear numerical simulations on RC frame buildings by means of FE models incorporating the features of the SPEAD system and the related mechanical behaviour. Beyond possible experimental studies, the application to real buildings can be very helpful in validating the proposed technique also from the point of view of the installation process, accounting for its advantages related to the need of works only from the outside and its drawbacks related to its possible applicability limits.

Conflict of interest

On behalf of all authors, the corresponding author states that there is no conflict of interest.

References

- [1] Rossetto T, Peiris N, Alarcon JE, So E, Sargeant S, Free M, Sword-Daniels V, Del Re D, Libberton C, Verrucci E et al. (2011) Field Observations from the Aquila, Italy Earthquake of April 6, 2009. *Bull Earthquake Eng* 9:11–37. <https://doi.org/10.1007/s10518-010-9221-7>
- [2] Masi A, Chiauzzi L, Santarsiero G, Manfredi V, Biondi S, Spacone E, Del Gaudio C, Ricci P, Manfredi G, Verderame GM (2018) Seismic response of RC buildings during the Mw 6.0 August 24, 2016 Central Italy earthquake: The Amatrice case study. *Bull Earthquake Eng* 17:5631–5654. <https://doi.org/10.1007/s10518-017-0277-5>
- [3] Loporcaro G, Cuevas A, Pampanin S, Kral MV (2018) Monotonic and low-cycle fatigue properties of earthquake-damaged New Zealand steel reinforcing bars. The experience after the Christchurch 2010/2011 earthquakes. *Procedia Structural Integrity* 11:194-201. <https://doi.org/10.1016/j.prostr.2018.11.026>
- [4] Gould PL, Goodno BJ, Gould NC, Caldwell P (2011) Behavior of Engineer Constructed Facilities in the Haitian Earthquake of January 12, 2010. *Procedia Engineering* 14:23-31. <https://doi.org/10.1016/j.proeng.2011.07.003>
- [5] Frascadore R, Di Ludovico M, Prota A, Verderame GM, Manfredi G, Dolce M, Cosenza E (2015) Local Strengthening of Reinforced Concrete Structures as a Strategy for Seismic Risk Mitigation at Regional Scale. *Earthquake Spectra*. 31(2):1083-1102. <https://doi.org/10.1193/122912EQS361M>
- [6] Di Ludovico M, Digrisolo A, Moroni C, Graziotti F, Manfredi V, Prota A, Dolce M, Manfredi G (2019) Remarks on damage and response of school buildings after the Central Italy earthquake sequence. *Bull Earthquake Eng* (2019) 17: 5679. <https://doi.org/10.1007/s10518-018-0332-x>
- [7] Manfredi V, Masi A (2017) Seismic strengthening and energy efficiency: towards an integrated approach for the rehabilitation of existing RC buildings. *Buildings* 8(3):36. <https://doi.org/10.3390/buildings8030036>
- [8] Santarsiero G, Masi A (2015) Seismic performance of RC beam–column joints retrofitted with steel dissipation jackets. *Engineering Structures* 85:95-106. <https://doi.org/10.1016/j.engstruct.2014.12.013>
- [9] Kazem Sharbatdar M, Kheyroddin A, Emami E (2012) Cyclic performance of retrofitted reinforced concrete beam–column joints using steel prop. *Construction and Building Materials* 36:287–294. <https://doi.org/10.1016/j.conbuildmat.2012.04.115>
- [10] Realfonzo R, Napoli A, Ruiz Pinilla JG (2014) Cyclic behavior of RC beam-column joints strengthened with FRP Systems. *Construction and Building Materials* 54:282–297. <https://doi.org/10.1016/j.conbuildmat.2013.12.043>
- [11] Sasmal S, Ramanjaneyulu K, Novák B, Srinivas V, Saravana Kumar K, Korkowski C, Roehm C, Lakshmanan N, Iyer NR (2011) Seismic retrofitting of nonductile beam-column sub-assembly using FRP wrapping and steel plate jacketing. *Construction and Building Materials* 25:175–182. <https://doi.org/10.1016/j.conbuildmat.2010.06.041>
- [12] Singh V, Bansal PP, Kumar M, Kaushik SK (2014) Experimental studies on strength and ductility of CFRP jacketed reinforced concrete beam-column joints. *Construction and Building Materials* 55:194–201. <https://doi.org/10.1016/j.conbuildmat.2014.01.047>
- [13] Attari N, Youcef YS, Amziane S (2019) Seismic performance of reinforced concrete beam–column joint strengthening by frp sheets. *Structures* 20:353-364. <https://doi.org/10.1016/j.istruc.2019.04.007>
- [14] Wang GL, Dai JG, Bai YL (2019) Seismic retrofit of exterior RC beam-column joints with bonded CFRP reinforcement: An experimental study. *Composite Structures* 224:111018. <https://doi.org/10.1016/j.compstruct.2019.111018>
- [15] Santarsiero G (2018) FE modelling of the seismic behavior of wide beam-column joints strengthened with CFRP systems. *Buildings* 8(2):31. <https://doi.org/10.3390/buildings8020031>

- [16] Del Vecchio C, Di Ludovico M, Prota A, Manfredi G (2016) Modelling beam-column joints and FRP strengthening in the seismic performance assessment of RC existing frames. *Composite Structures* 142:107-116. <https://doi.org/10.1016/j.compstruct.2016.01.077>
- [17] Wang X., Zhou C., Ai J., Petru M., Liu Y., (2020) Numerical investigation for the fatigue performance of reinforced concrete beams strengthened with external prestressed HFRP sheet, *Construction and Building Materials* 237:117601, <https://doi.org/10.1016/j.conbuildmat.2019.117601>.
- [18] Zhu Y., Zhang Y., Hussein H. H., Chen G.,(2019) Numerical modeling for damaged reinforced concrete slab strengthened by ultra-high performance concrete (UHPC) layer, *Engineering Structures*, 110031, <https://doi.org/10.1016/j.engstruct.2019.110031>.
- [19] Masi A, Santarsiero G (2013) Seismic Tests on RC Building Exterior Joints with Wide Beams. *Advanced Materials Research* 787:771-777. <https://doi.org/10.4028/www.scientific.net/AMR.787.771>
- [20] Masi A, Santarsiero G, Nigro D (2013) Cyclic tests on external RC beam-column joints: role of seismic design level and axial load value on the ultimate capacity. *Journal of Earthquake Engineering* 17(1):110-136. <https://doi.org/10.1080/13632469.2012.707345>
- [21] Ordinance of the President of the Council of Ministers (OPCM) 20 March 2003, n.3274, “Primi elementi in materia di criteri generali per la classificazione sismica del territorio nazionale e di normative tecniche per le costruzioni in zona sismica”, Official Journal, General serie n.105, 08-05-2003 – Ordinary Supplement n. 72 (in Italian), available at www.gazzettaufficiale.it
- [22] CEN (2005). EN 1998-3:2005 Eurocode 8: Design of structures for earthquake resistance - Part 3: Assessment and retrofitting of buildings
- [23] Ministry Decree 17 gennaio 2018, “Aggiornamento delle «Norme tecniche per le costruzioni»”, Official Journal, General serie n.42, 20-02-2018 – Ordinary Supplement n. 8 (in Italian), available at www.gazzettaufficiale.it
- [24] CEN (2004). EN 1998-1:2004 Eurocode 2 - Design of concrete structures - Part 1: General rules and rules for buildings
- [25] Cervenka Consulting, 2000-2014. ATENA Program Documentation, Part 1, ATENA Theory Manual
- [26] Hordijk DA (1991) Local Approach to Fatigue of Concrete. Dissertation, Delft University of Technology, The Netherlands, ISBN 90/9004519-8
- [27] MC10. CEB-FIP Model Code 2010. Comité Euro-International du Béton; 2010
- [28] MC90. CEB-FIP Model Code 1990. Comité Euro-International du Béton; 1993
- [29] Jendele L, Cervenka J (2006) Finite element modeling of reinforcement with bond. *Computers & Structures* 84(28):1780-1791. <https://doi.org/10.1016/j.compstruc.2006.04.010>
- [30] Masi A, Santarsiero G, Lignola GP, Verderame GM (2013) Study of the seismic behaviour of external RC beam-column joints through experimental tests and numerical simulations. *Engineering Structures* 52:207–219. <https://doi.org/10.1016/j.engstruct.2013.02.023>
- [31] Campione G (2015) Analytical prediction of load deflection curves of external steel fibers R/C beam-column joints under monotonic loading. *Engineering Structures*, 83:86-98. <https://doi.org/10.1016/j.engstruct.2014.10.047>
- [32] Ronagh HR, Baji H (2014) On the FE Modeling of FRP-Retrofitted Beam-Column Subassemblies. *Int J Concr Struct Mater* 8:141–155. doi:10.1007/s40069-013-0047-y